CHEMISTRY OF MATERIALS

pubs.acs.org/cm

Article

Reactant-Dependent, $10^8\times$ Conductivity Modulation in Plasma-Enhanced Atomic Layer Deposition for Black TiO_2 Films

S. Novia Berriel, Terrick McNealy-James, Taylor M. Currie, Eric Bissell, Brian Butkus, Chien-Hsuan Chen, Luis Tomar, Jacob Baillie, Daniel R. Gamelin, Kristopher O. Davis, Titel Jurca, and Parag Banerjee*

Cite This: https://doi.org/10.1021/acs.chemmater.4c00667

Read Online

ACCESS | Metrics & More | Article Recommendations | Supporting Information

ABSTRACT: A rational choice of reactants during plasma-enhanced atomic layer deposition (PEALD) can lead to extreme changes in film properties. Herein, we demonstrate with this approach, a $10^8\times$ change in electrical conductivity of an insulating TiO_2 film to a highly conducting TiO_2 film. The films are deposited using PEALD of titanium tetraisopropoxide (TTIP) with a 300 W plasma containing 5% H_2 in argon as a reactant at 200 °C. The growth and film characteristics are compared to the ALD of TiO_2 films grown using widely reported processes involving H_2O and O_2 plasma as reactants. *In situ* ellipsometry is used to extract the growth per cycle (GPC) of the TTIP + H_2 plasma process, which is 0.013 nm/cycle. This can be compared to the GPC of 0.011 and 0.034 nm/cycle for the TTIP + H_2O and TTIP + O_2 plasma processes, respectively. X-ray photoelectron spectroscopy of the TTIP + H_2 plasma films shows a reduced state, with a Ti^{3+}/Ti^{4+} ratio of 72%, compared to 23.4 and 29.6% for the TTIP + H_2O and TTIP + O_2 plasma processes, respectively. The TTIP + H_2 plasma film is amorphous as-deposited and has a root-mean-square surface roughness of 1.42 nm. The film demonstrates an apparent optical bandgap of 3.77 eV and strong free carrier absorption in the near-infrared. The room temperature resistivity of the film is measured to be 67 mΩ cm, with an activation energy for conduction of 0.142 eV and a free electron carrier concentration of 7.89×10^{21} cm^{-3}. The TTIP + H_2 plasma process makes the reduced TiO_2 film appear "black" in color.

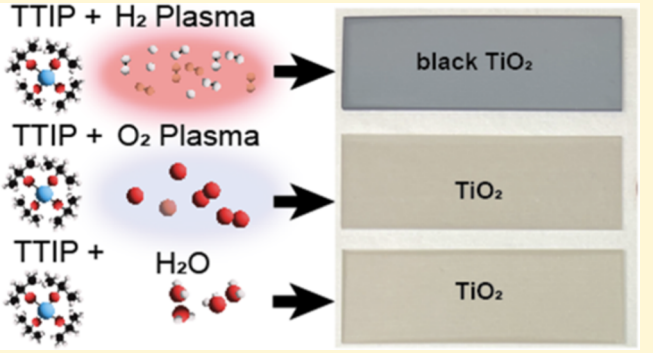

1. INTRODUCTION

Titanium dioxide (TiO_2) is a widely used metal oxide employed for photoelectrochemical water splitting,[1] dye-sensitized solar cells,[2] white pigments,[3] and as a UV absorber in sunscreens.[4] TiO_2, however, is limited in certain applications due to its wide bandgap (3.3 eV) and poor electrical conductivity. "Black" titania[5−9] is a name given to disordered TiO_2 in its heavily reduced state (TiO_{2-x}). Black titania in powder form can come in colors from yellow and beige to blue and black, as oxygen vacancies are introduced into the crystal structure.[10] The unique form of black titania is characterized by its color, increased conductivity, narrower bandgap, and high optical absorbance from the UV to the near-infrared (NIR). Accordingly, black titania has been used as a light-absorbing layer in solar cells,[11] an electrode for photocatalytic H_2 generation,[8,12] a photocatalyst for removal of environmental pollutants such as dyes and organic pollutants,[10,11] as well as an electrode for lithium-ion batteries.[13]

To date, black titania has been synthesized in various forms, such as core−shell nanoparticles using high-pressure hydrogen thermal treatment[5,14] and thin films using hydrogen and/or nitrogen plasma treatment of an otherwise stoichiometric TiO_2 film.[15] Often, black titania is synthesized by treating TiO_2 with dopants such as nitrogen and hydrogen or by aggressively reducing to incorporate oxygen vacancies.[10,16,17] As TiO_2 nanoparticles are commercially available, it is common for black titania to be synthesized or derived in nanoparticle form.[11,18,19] Other forms of black titania are reported and include nanowires[20] and nanotubes.[12,21]

Films of black titania are usually formed by using a two-step process. First, the films are deposited as stoichiometric TiO_2. Subsequently, (1) a hydrogen anneal environment,[14] (2) an O_2-deficient environment, or (3) a hollow cathode hydrogen plasma[22] is used to reduce the TiO_2. The resulting TiO_{2-x} films are amorphous due to high defect concentration and have low resistivity. These defects also cause a narrowing of the bandgap in the titania and produce a darker color, widening

Received: March 6, 2024
Revised: August 1, 2024
Accepted: August 1, 2024

the absorption window to the visible and IR.[10] However, the deposition of black titania directly, and as a single-step process, is far less common. The work of Ali-Löytty *et al.*, is one example for which black titania is deposited directly by atomic layer deposition (ALD).[23]

ALD is a technique by which films are deposited using an alternating sequence of self-limiting surface reactions.[24] The deposition is consequently highly conformal with precise monolayer control of the thickness. Further, plasma can be incorporated into ALD processes to induce surface reactions at lower temperatures or to produce cleaner films with lower contaminants. These processes are known as "plasma-enhanced" ALD (PEALD).[25−28]

There is extensive work[29−34] demonstrating the ALD and PEALD of TiO_2. The commonly used precursors include titanium tetrachloride ($TiCl_4$), tetrakis(dimethylamido)-titanium(IV) (TDMAT, with formula $Ti[N(CH_3)_2]_4$), and titanium tetraisopropoxide (TTIP, with formula $Ti[OC_3H_7]_4$); the former two precursors contain no oxygen and the latter contains Ti−O bonds. The amount of control that an ALD process provides enables a fine degree of composition and crystallinity tuning of the film. With this approach, black titania films have been prepared using TDMAT and water.[23] However, the black titania reported has a relatively low conductivity of ∼150 S/m, compared to Wang *et al.*,[11] of 21,671 S/m for films prepared using magnetron sputtering. Our hypothesis for the observed low conductivity in ALD black titania pertains to the choice of the precursor—TDMAT—which contains the Ti−N bond. Second, the use of H_2O as a reactant is not ideal, as it does not produce the aggressively reducing conditions required for the synthesis of black titania.

Therefore, in this study, we propose the use of TTIP and H_2 plasma as a viable PEALD method to produce black titania in a single processing step. This choice of chemistry provides certain advantages. First, the precursor TTIP is chosen to take advantage of the existing Ti−O bonds in the molecule. Next, as a reactant, we use H_2 plasma, the primary purpose of which is to create highly activated H-species that can reduce the film after each cycle of deposition. Additionally, the presence of plasma can help deposit a cleaner film with minimal carbon contamination. We investigate the film properties and morphology through X-ray photoelectron spectroscopy (XPS), Raman spectroscopy, atomic force microscopy (AFM), UV−vis spectroscopy, temperature-dependent electrical measurements, and Hall measurements. We further compare our black titania films to TiO_2 films deposited by using water and O_2 plasma as reactants in order to demonstrate the effect of the H_2 plasma reactant on the film properties. Our results highlight the ease of synthesis of high-quality ALD-based black titania with the right choice of precursor and reactant chemistry.

2. EXPERIMENTAL SECTION

2.1. Synthesis Techniques. ALD of titania films was carried out on a Veeco Fiji Gen2 ALD system with a remote plasma source. An Ebara E30W pump (pumping speed 3000 L/min) was used for generating a vacuum with an ultimate chamber base pressure of 60 mTorr. The deposition temperature for all processes was 200 °C. For the first process TTIP + H_2O, the TTIP was pulsed for 0.06 s followed by a 4 s Ar purge, a 0.06 s water pulse, and another 4 s Ar purge. For consistent metal precursor dosing, the TTIP + H_2 plasma then consisted of a 0.06 s pulse of TTIP and a 10 s Ar purge followed by a 5 s plasma exposure of 300 W plasma of Ar−H_2 5%, and a 6 s purge. Lastly, the TTIP + O_2 plasma process consisted of a 0.06 s pulse of TTIP and a 10 s Ar purge followed by a 5 s plasma exposure of 300 W plasma of O_2, and a 6 s purge. The saturation curves for all processes are provided in Supporting Information S1. We chose the pulse and purge times to be undersaturated to deliberately create partially reducing conditions for the film with the aim of improving the electronic conductivity. Film thicknesses were monitored via *in situ* spectroscopic ellipsometry using a Woollam M2000 ellipsometer. Final thicknesses of the three films varied from 20 to 40 nm and are noted when describing specific characterization results.

2.2. Characterization Techniques. XPS was performed on a Fisher Scientific ESCALAB 250Xi instrument using Al Kα (1486.6 eV) as the X-ray source. All acquisitions were acquired using charge compensation; spectra were acquired pre and post 60 s Ar^+ ion etching (400 eV) to remove adventitious carbon from the sample surface. Survey spectra were recorded with a pass energy of 150 eV, a step size of 1 eV, and a dwell time of 50 ms. The fine spectra were recorded with a pass energy of 20 eV, a step size of 0.10 eV, and a dwell time of 50 ms. The spot size used for the acquisition was 650 μm. The number of scans per spectrum ranged from 5 to 15 to adjust for the optimal signal-to-noise ratio. All spectra were calibrated to the C 1s peak located at 284.8 eV.

Raman was performed using a HORIBA LabRAM HR Evolution Nanoconfocal Raman system. Data were collected using a 785 nm laser at 25 mW over a spot size of 4 μm (50× objective), using a grating of 300 gr/mm, for 10 accumulations each with a 30 s integration time. AFM was performed in tapping mode on a Park System NX10, with Bruker cantilever RTESPA (resonance frequency: 329−372 kHz; force constant: 20−80 N/m). AFM data was processed in the open-source software Gwyddion. Absorption measurements were performed with a Shimadzu UV-3600i Plus UV−vis−NIR spectrophotometer by using an internal diffuse reflectance accessory for solid-state sample measurements.

To extract the temperature-dependent conductivity of titania films deposited under different conditions, the transmission line method (TLM) was used. TLM test structures were fabricated through e-beam evaporation. Ag TLM pads were deposited on top of grown 40 nm titania films with a target thickness of 200 nm and a deposition rate of 0.1 nm/s. An MDC I−V plotter featuring a temperature control chuck was used to extract resistance values between contact pads with different spacing. The sheet resistance (R_{sh}) of films was then determined from the slope of TLM plots. With the extracted R_{sh} under different testing temperatures, both the temperature-dependent resistivity and conductivity were then calculated accordingly.

Hall measurements were conducted on the samples using a JanisST500-1-2CX commercial probe station with gold-plated tungsten probe tips of 200 μm tip diameter. Indium dots were pressed into the four corners of the film to serve as electrodes for probe placement. Hall measurements were performed under magnetic fields of 0.2135 and −0.2135 T.

3. RESULTS AND DISCUSSION

3.1. Growth Characteristics. Figure 1 shows *in situ* spectroscopic ellipsometry data with the variation of film thickness on a Si wafer as a function of cycle numbers for the three processes described. Growth is immediate upon starting the process, thus indicating no incubation. The average slope of the thickness vs ALD cycles can be used to estimate the growth per cycle (GPC, in nm/cy) of the three processes. The TTIP + H_2O process shows the lowest GPC at 0.011 nm/cy. This value can be compared to Ritala *et al.*,[35] who report a GPC of 0.016 nm/cy. The TTIP + O_2 plasma GPC is the highest at 0.034 nm/cy. This value is in line with those reported by Aghaee *et al.*,[36] of 0.037−0.057 nm/cy. Finally, the TTIP + H_2 plasma has a growth rate between the O_2 and H_2O processes with a GPC of 0.013 nm/cy. No prior GPC reports of this process are available.

https://doi.org/10.1021/acs.chemmater.4c00667
Chem. Mater. XXXX, XXX, XXX−XXX

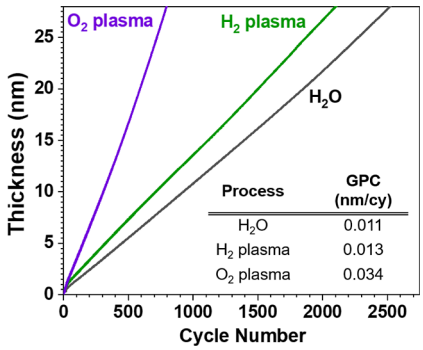

Figure 1. *In situ* spectroscopic ellipsometry data showing thickness vs ALD cycle numbers for three processes (i) TTIP + H_2O, (ii) TTIP + H_2 plasma, and (iii) TTIP + O_2 plasma processes. The inset table lists the GPC of the three processes.

Representative zoomed images (consisting of ~4 ALD cycles) of the growth curves of the three processes are shown in Figure 2 where changes to film thickness are provided as a function of time. The snapshots of the growth are obtained under steady-state conditions (i.e., linear regime of the growth curve from Figure 1). The H_2O process (Figure 2A) is relatively fast, as can be seen in the lesser number of data points collected per ALD cycle. The H_2 plasma (Figure 2B) and the O_2 plasma (Figure 2C) processes are relatively longer and result in a larger set of data points collected during each cycle. We define Δ_1 (nm) as the growth upon TTIP exposure and Δ_2 (nm) as the ligand removal reaction upon exposure to the reactant. Thus, $(\Delta_1 - \Delta_2)$ is the GPC at the granularity level of a single pulse. While slight variations to $(\Delta_1 - \Delta_2)$ are to be expected, we show examples where $(\Delta_1 - \Delta_2)$ is close to the global (i.e., average) GPC.

The cyclic variation of Δ_1, Δ_2, and $(\Delta_1 - \Delta_2)$ are shown in Table 1 for all three processes. It can be seen that during the TTIP + H_2O process, the TTIP adsorption causes an increase in thickness of 0.056 nm, while upon H_2O pulse, a drop in thickness of 0.045 nm is observed. Thus, the GPC is 0.011 nm/cycle. The TTIP + H_2 plasma has a similar gain and loss of thickness (0.056 and 0.043 nm, respectively) and a resultant GPC of 0.013 nm/cycle. On the other hand, the TTIP + O_2 plasma process shows higher gains and losses in thickness during the TTIP pulse and reactant pulse. Here, the TTIP adsorption step causes a thickness gain of Δ_1 of 0.234 nm. This gain in thickness is 4.2× more than the thickness gain from the TTIP adsorption step in the H_2O process. The loss of thickness upon O_2 plasma exposure is 0.200 nm and is ~4.4× more than the thickness loss from the reaction step in the H_2O process. Overall, these thickness gains and losses lead to a higher GPC of 0.034 nm/cy, which is 3.1× higher than the H_2O process.

Table 1. Three Processes—TTIP + H_2O, TTIP + H_2 Plasma, and TTIP + O_2 Plasma, and Their Individual Δ_1, Δ_2, and $(\Delta_1 - \Delta_2)$ Are Provided[a]

Process	Δ_1 (nm)	Δ_2 (nm)	GPC (nm/cy) $\Delta_1 - \Delta_2$
H_2O	0.056	0.045	0.011
H_2 plasma	0.056	0.043	0.013
O_2 plasma	0.234	0.200	0.034

[a]Data extracted from Figure 2.

3.2. Film Composition. The surface compositions of the three TiO_2 films were analyzed using XPS. Peak deconvolution and assignments are provided in Supporting Information Figure S2. Here, we focus on the primary and comparative results. In Figure 3A, the C fine spectra (calibrated with C 1s centered at 284.8 eV) are shown—where all spectra are obtained after 60 s of Ar^+ sputtering to eliminate any effects from adventitious carbon. The results indicate that the TTIP + H_2O process has the highest carbon content among the three processes (4.5 at. %). The broadening of the C peak toward higher binding energy (BE) is indicative of C−O and C═O bonds. Both TTIP + H_2 plasma and TTIP + O_2 plasma have lower, but similar, carbon content (2.6 at. %). These results are summarized in Table 2. Our C 1s XPS results are in line with published reports on TTIP based ALD TiO_2 films.[36−38] It is known that H_2O as a reactant leaves more carbon in the resulting film than a sufficient dose of O_2 plasma.[37] The O fine spectra is shown in Figure 3B, deconvoluting into two peaks (Supporting Information Figure S2): one at 530.1 eV corresponding to the O^{2-} state of oxygen in TiO_2 and another shoulder at the higher BE of 531.5 eV corresponding to surface adsorbed hydroxyl groups.[39,40]

The Ti 2p fine spectra are shown in Figure 3C. For the three films, the Ti $2p_{3/2}$ is centered at a BE of 458.8 ± 0.09 eV and represents the Ti^{4+} oxidation state.[39,41] All samples also showed a shoulder on the lower BE side at 457.2 ± 0.05 eV (Supporting Information Figure S2). This peak is attributed to the Ti^{3+} state.[39,41] The strongest shoulder observed is for the

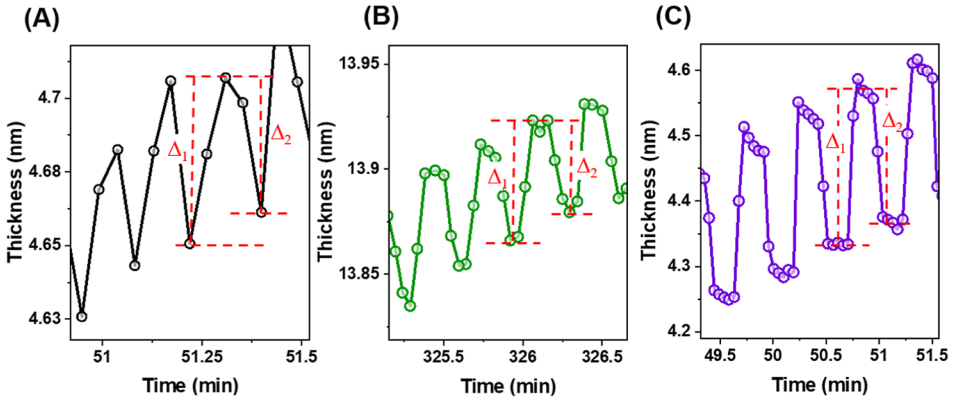

Figure 2. Higher time resolution *in situ* spectroscopic ellipsometry growth rate data for (A) TTIP + H_2O, (B) TTIP + H_2 plasma, and (C) TTIP + O_2 plasma processes. Individual TTIP adsorption gain and reaction loss in thickness are labeled as Δ_1 and Δ_2, respectively.

https://doi.org/10.1021/acs.chemmater.4c00667
Chem. Mater. XXXX, XXX, XXX−XXX

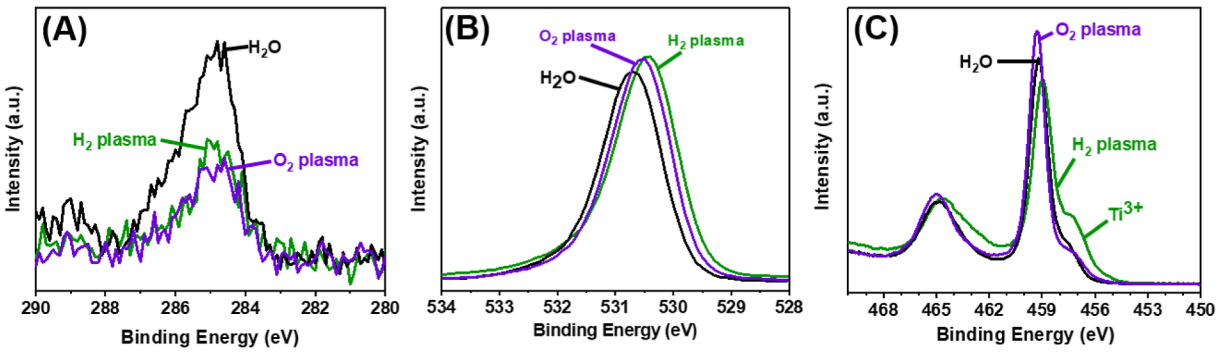

Figure 3. XPS data of the three films prepared using TTIP + H_2O, TTIP + H_2 plasma, and TTIP + O_2 plasma showing (A) C 1s, (B) O 1s, and (C) Ti 3d fine spectra.

Table 2. Atomic % Carbon, O/Ti Ratio, and Ti^{3+}/Ti^{4+} (%) Obtained from XPS

process	C at. %	O/Ti	Ti^{3+}/Ti^{4+} (%)
H_2O	4.5	1.80	23.4
H_2 plasma	2.6	1.79	72.0
O_2 plasma	2.6	1.89	29.6

TTIP + H_2 plasma process and indicates that the film is strongly reduced.

From the deconvolution analyses of the O and Ti fine spectra, the O/Ti and Ti^{3+}/Ti^{4+} ratios can also be estimated. This is given in Table 2. We note that the O/Ti ratio varies depending on the phase of titania.[42] For example, for rutile TiO_2 the O/Ti is 2.00, and for the anatase phase, the ratio is 1.90. For the three samples, the measured O/Ti ratio varies from 1.79 for TTIP + H_2 plasma to 1.89 for the TTIP + O_2 plasma. Further, Ti^{3+}/Ti^{4+} can also be obtained from the XPS analyses. For the TTIP + H_2O sample, this value is 23.4% while for the TTIP + O_2 plasma sample, this value is 29.6%. The TTIP + H_2 plasma sample shows a Ti^{3+}/Ti^{4+} of 72%. This result can be compared to the 30 nm ALD black titania results from Ali-Löytty *et al.*,[23] who report a Ti^{3+}/Ti^{4+} ratio of ∼1.0% and an O/Ti ratio between 1.9 and 2.0. For a sputtered ∼460 nm TiO_2 films post treated with hollow cathode H_2 plasma, Godoy *et al.*[22] report a $(Ti^{2+} + Ti^{3+})/Ti^{4+}$ ratio of 36%.

3.3. Phase and Structural Characteristics. Further structural characterization was conducted on the 30 nm thick films, including Raman spectroscopy as shown in Figure 4A. The TTIP + H_2O and TTIP + H_2 plasma films were amorphous and had broad peaks at 364 and 559 cm^{-1}. On the other hand, the TTIP + O_2 plasma film shows a sharp peak at 144 cm^{-1} corresponding to the anatase phase.[43] The presence of anatase is further confirmed by grazing incidence X-ray diffraction in supporting evidence (Supporting Information Figure S3). The AFM area scans for the three 30 nm films—TTIP + H_2O, TTIP + H_2 plasma, and TTIP + O_2 plasma—are shown in Figure 4B–D, respectively. The film root-mean-square (rms) surface roughness values for all three films are shown in Figure 4E. The TTIP + H_2O rms roughness is 0.54 nm and the TTIP + H_2 plasma rms roughness is 1.42 nm. The

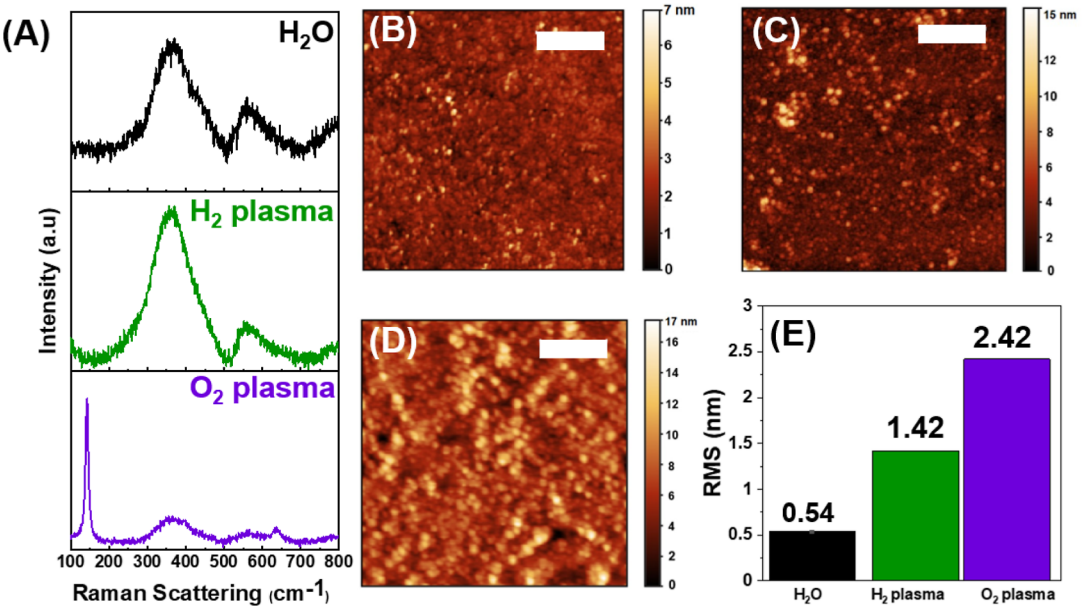

Figure 4. (A) Raman data for the three films (∼30 nm in thickness). While H_2O and H_2 plasma shows an amorphous nature, the O_2 plasma is crystalline, with the anatase peak at 144 cm^{-1}. The AFM image shows the (B) TTIP + H_2O process, (C) TTIP + H_2 process, and (D) TTIP + O_2 plasma process. Scale bar: 500 nm. (E) rms roughness of the three films shows the O_2 plasma film with the highest roughness, whereas the H_2O process has the lowest roughness.

https://doi.org/10.1021/acs.chemmater.4c00667
Chem. Mater. XXXX, XXX, XXX−XXX

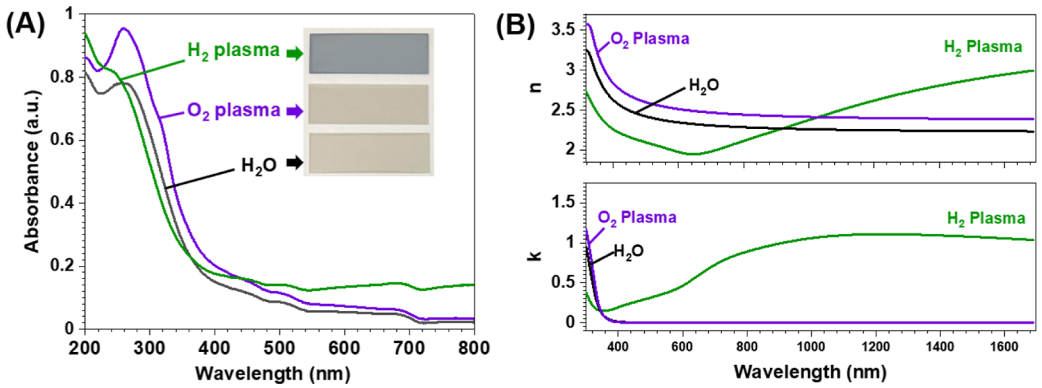

Figure 5. (A) UV−vis absorbance of TiO_2 prepared using TTIP + H_2O, TTIP + H_2 plasma, and TTIP + O_2 plasma. All films were ∼30 nm in thickness. The H_2 plasma TiO_2 film shows a higher absorbance for wavelength $\lambda > 500$ nm. The inset shows coated microscope slides of the same. (B) Refractive index "n" and extinction coefficient "k" for the three films obtained via spectroscopic ellipsometry.

TTIP + O_2 plasma film, which is a crystalline anatase phase, has the highest roughness at 2.42 nm.

3.4. Optical and Electronic Properties. UV−vis spectroscopy (200−800 nm) was conducted on the three films deposited on quartz substrates. These data are shown in Figure 5A. Corresponding Tauć plots (Supporting Information Figure S4) allow extraction of bandgaps of ∼3.5−3.7 eV for all three films, in line with reported values for titania thin films.[23,44] While this bandgap is larger than is often reported for black titania, it is in line with reported increase of apparent bandgap for highly conducting titania films.[23,45] The wider bandgap is attributed to the Moss−Burstein effect,[46] whereby the increase in free carriers populates states near the conduction band edge. Further, a higher absorbance is observed for the TTIP + H_2 plasma film towards the NIR region. The inset shows the optical images of the glass slides with 30 nm films deposited from the three processes. While the TTIP + H_2O and TTIP + O_2 plasma samples show light beige but optically transparent films, the TTIP + H_2 plasma film is markedly darker in color, in line with the higher absorbance observed in the UV−vis data. In this sense, the TTIP + H_2 plasma film can be termed as "black titania".

In Figure 5B, the refractive index "n" and extinction coefficient "k" are shown across a wider spectrum (320−1680 nm), as extracted from spectroscopic ellipsometry measurements of the 30 nm films. As a point of reference, "n" for the three films (TTIP + H_2O, TTIP + H_2 plasma, TTIP + O_2 plasma) extracted at 633 nm are 2.33, 1.95, and 2.50, respectively. These values appear to be in the range of values reported for TiO_2 films.[47,48] The TTIP + H_2 plasma sample has a large Drude-like absorbance tail that extends well into the NIR. This is indicative of free carrier absorption in the film.

To confirm the presence of free carriers, temperature-dependent conductivity measurements were performed on 40 nm thick films. The data are shown in Figure 6. Film conductivity for all three films increased with temperature, indicating a thermally activated conduction mechanism as is expected of semiconductors. The room temperature (25 °C) conductivity for the TTIP + H_2O film was 4.06×10^{-5} S/m (2.46 MΩ cm), and for the TTIP + O_2 plasma film, it was 8.72×10^{-5} S/m (1.15 MΩ cm). This shows that the under-saturated conditions employed for the processes did not result in a conductivity enhancement. In contrast, the TTIP + H_2 plasma film had a room temperature conductivity of 19.55×10^3 S/m (5.12 mΩ cm). This value is 5×10^8 times the

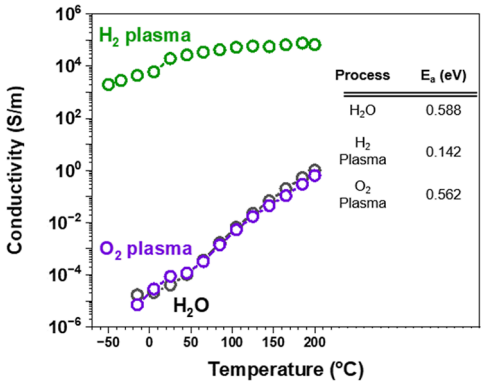

Figure 6. Temperature-dependent conductivity measurements for 30 nm films of (i) TTIP + H_2O, (ii) TTIP + H_2 plasma, and (iii) TTIP + O_2 plasma. The inset table shows the activation energy for conduction.

conductivity obtained for the TTIP + H_2O or TTIP + O_2 plasma films. The value is also greater than that reported by Ali-Löytty *et al.*, of ∼150 S/m for a 30 nm thick film.

When there is a linearity of the log of conductivity with respect to inverse temperature,[49−51] an Arrhenius-type thermally activated conduction mechanism can be used to model the conductivity of insulators and wide band gap semiconductors, as shown in Figure 6. Using the equation for conduction (σ), given as $\sigma = \sigma_o e^{-E_a/k_B T}$, where E_a is the activation energy, k_B is Boltzmann's constant, and T is the temperature in Kelvin, the activation energy for conductivity was obtained and is provided in the inset Table of Figure 6. In these measurements, all films had a 40 nm thickness. Both the TTIP + H_2O and TTIP + O_2 plasma films have similar activation energy of 0.588 and 0.562 eV, respectively. In contrast, the TTIP + H_2 plasma film has a much lower activation energy of 0.142 eV, indicating that the film is conducting due to its reduced state. The increased conductivity is related to generation of oxygen vacancies, which provide donor-like states in the bandgap that are close to the conduction band edge of TiO_2.

Room temperature Hall measurements were conducted on 20 nm thick samples. Due to the relatively high resistance of the TTIP + H_2O and TTIP + O_2 plasma films, no Hall data could be reliably obtained for these films. The results for the conducting TTIP + H_2 plasma film are provided in Table 3. For a room temperature resistivity of 67 mΩ cm (1492 S/m),

https://doi.org/10.1021/acs.chemmater.4c00667
Chem. Mater. XXXX, XXX, XXX−XXX

Table 3. Room Temperature Hall Measurements of the TTIP + H_2 Plasma Film and Its Comparison with Black Titania Films Reported by Others[a]

	deposition technique	film thickness (nm)	carrier mobility ($cm^2/(V\ s)$)	electron density (cm^{-3})	resistivity (mΩ cm)
this work	ALD (w/TTIP)	20	1.77×10^{-2}	7.89×10^{21}	67
Ali-Löytty *et al.*	ALD (w/TDMAT)	30	not given	not given	667
Lü, *et al.*	PLD	37	2.0	0.32×10^{20}	300
Wang *et al.*	magnetron sputtering	663	not given	7.80×10^{20}	4.6

[a](Ali-Löytty *et al.*,[23] Lü *et al.*,[52] Wang *et al.*,[11]).

an electron carrier concentration of 7.89×10^{21} cm^{-3} and a carrier mobility of 1.77×10^{-2} cm^2/V s are obtained. A comparison with the black titania films obtained by Ali-Löytty *et al.*,[23] Lü *et al.*,[52] and Wang *et al.*[11] are also provided. The PEALD black titania reported in our work has one of the lowest resistivities and a high carrier concentration for a thickness of only 20 nm.

4. DISCUSSION

The collective *in situ* process data and ex situ characterization data provide insights into the growth mechanisms of the three processes. The TTIP + H_2O process at 200 °C shows a GPC of 0.011 nm/cy and Δ_1 and Δ_2 as 0.056 and 0.045 nm, respectively. The GPC is low compared to other literature reports. The low GPC is a deliberate attempt to undersaturate the process, creating reducing conditions during the TTIP + H_2O process. Rahtu and Ritala[53] have suggested that half the ligands associated with an adsorbed TTIP are effectively removed during the H_2O pulse. However, it has been shown recently that −iPr ligands from TTIP can be incorporated in the TiO_2 films.[54] Surface reaction modeling indicates that a combination of hydrolysis and pyrolytic decomposition of TTIP may occur during the film growth.[55] Both reaction pathways are time- and temperature-dependent. Our XPS data show substoichiometric O/Ti ∼ 1.80 and a high 4.5 at. % C, in the film in line with an undersaturated process.

The TTIP + O_2 plasma process at 200 °C demonstrates the highest growth rate of 0.034 nm/cy with high Δ_1 and Δ_2 of 0.234 and 0.200 nm, respectively. According to Rai and Agarwal,[56] the high growth rate of TTIP + O_2 plasma process is due to the hydroxyl and metal−carbonate species that are formed on the growth surface during an O_2 plasma step; both species aid in the adsorption of TTIP. This is in line with the O/Ti ratio of 1.89 obtained with XPS, which is the highest among the three processes. This also explains the high Δ_1 observed. A correspondingly high Δ_2 is expected as the O_2 plasma can generate combustion byproducts of the −iPr ligand. A GPC of 0.083 nm/cy is reported by Rai *et al.*, which is higher than the GPC reported in the present work. This discrepancy can be understood by recognizing the different residence times of reactants due to hardware differences and different deposition temperatures (150 °C for Rai *et al.*, vs 200 °C in the present work). Additionally, we note that the deposited film is anatase. Film crystallinity can also play an important role in enhancing GPCs.[57]

The TTIP + H_2 plasma process at 200 °C shows a GPC of 0.013 nm/cy with Δ_1 and Δ_2 values of 0.056 and 0.043, respectively. The O/Ti is the lowest at 1.79, and the Ti^{3+}/Ti^{4+} is significantly high at 72%. This indicates that the H_2 plasma (noting that the plasma is created using Ar with 5% H_2) reduces the metal center. We propose two primary species in a H_2 plasma—protons (H^+) and atomic hydrogen (H*), responsible for the above effects.[58] Both species attack the electron-rich O in TTIP: $Ti-[O-CH(CH_3)_2]_4$, but from different sides. The electrophilic attack of H^+ is on the O−C bond. The −iPr ligand releases propane (and other alkanes), leaving a Ti−OH surface group. On the other hand, H* attacks the Ti−O bond, releases isopropanol, and reduces Ti^{4+} to Ti^{3+}. A similar surface reaction has been observed during dissociation of TTIP on a catalytically active Pt substrate.[59] The above reaction pathways are also consistent with the XPS data, which shows low C content of the TTIP + H_2 plasma films.

Based on the reaction mechanism proposed above, the defect chemistry responsible for the high electrical conductivity of the black titania can be explained as follows: the removal of O from the TiO_2 can be represented using Kroger−Vink notation as, $xO_O^{\times} \rightarrow xV_O^{\circ\circ} + 2xe^- + \frac{x}{2}O_2\uparrow$ where, x represents the moles of O removed from the TiO_2 lattice resulting in the availability of $2x$ electrons. These electrons can be localized at various defects within the band gap of TiO_2. A neutral oxygen vacancy ($V_O^{\times}$) suggests that the 2 electrons generated are localized on the defect. On the other hand, $V_O^{\circ\circ}$ releases the 2 electrons. *Ab initio* calculations of amorphous TiO_2 show that $V_O^{\times}$ forms deep, midgap states, while $V_O^{\circ\circ}$ defects form closer to the conduction band edge.[60] When the electron is localized in the vicinity of a Ti^{4+} site, the following reaction is expected, $yTi_{Ti}^{\times} + ye^- \rightarrow yTi_{Ti}'$. Represented another way, y moles of electrons are expected to reduce y moles of Ti^{4+} to Ti^{3+}. Here, x and y are independent parameters, yielding varying degrees of O/Ti content and Ti^{3+}/Ti^{4+} ratios.

Given that the O/Ti and Ti^{3+}/Ti^{4+} can be obtained with XPS, we perform these specific calculations for the TTIP + H_2 plasma film. One obtains for an O/Ti = 1.79 (from Table 2), x = 0.21. Thus, the total mole fraction of generated electrons = 0.42. Next, for a $Ti^{3+}/Ti^{4+} = 0.72 = y/(1-y)$. Solving for y, we obtain y = 0.42. Thus, XPS data remarkably suggest that all electrons generated because of the removal of O are utilized to reduce $Ti^{4+} \rightarrow Ti^{3+}$ and participate in the conduction process. This electronic state appears to be close to the conduction band edge with an $E_a \sim 0.142$ eV and is responsible for the $10^8\times$ conductivity enhancement of the TTIP + H_2 plasma film.

5. CONCLUSIONS

By rationally choosing the metal precursor that contains an existing Ti−O bond and a corresponding reactant that is highly reducing, we have successfully demonstrated the PEALD of 20−40 nm thick, highly conducting, and reduced black titania thin films. Using titanium tetraisopropoxide ($Ti[OC_3H_7]_4$) and 5% H_2 + Ar plasma as a reactant, black titania films were deposited at 200 °C with a GPC of 0.013 nm/cycle. Film stoichiometry was determined to be $TiO_{1.79}$, where the Ti^{3+}/Ti^{4+} ratio is 72% as determined by XPS. The film is amorphous

https://doi.org/10.1021/acs.chemmater.4c00667
Chem. Mater. XXXX, XXX, XXX−XXX

in nature with a rms surface roughness of 1.42 nm and a measured optical band gap of ~3.77 eV. Strong free carrier absorption is observed in the NIR. Room temperature electrical resistivity in a 20 nm black titania film is determined to be 67 mΩ cm with a free electron carrier concentration of 7.89×10^{21} cm^{-3}. The availability of a PEALD technique for depositing black titania films provides opportunities for its application in solid-state devices, solar cells, and battery electrodes.

■ ASSOCIATED CONTENT

Supporting Information

The Supporting Information is available free of charge at https://pubs.acs.org/doi/10.1021/acs.chemmater.4c00667.

ALD saturation curves for TTIP + H_2O, TTIP + H_2 plasma, and TTIP + O_2 plasma processes, deconvoluted XPS spectra of O 1s and Ti 2p, grazing incidence XRD for all three films, and Tauć plots of TiO_2 films (PDF)

■ AUTHOR INFORMATION

Corresponding Author

Parag Banerjee − *Department of Materials Science and Engineering, University of Central Florida, Orlando, Florida 32816, United States; Florida Solar Energy Center, University of Central Florida, Cocoa, Florida 32922, United States; Nano Science and Technology Center and REACT Faculty Cluster, University of Central Florida, Orlando, Florida 32816, United States;* orcid.org/0000-0003-0401-8155; Email: parag.banerjee@ucf.edu

Authors

S. Novia Berriel − *Department of Materials Science and Engineering, University of Central Florida, Orlando, Florida 32816, United States*

Terrick McNealy-James − *Department of Physics, University of Central Florida, Orlando, Florida 32816, United States;* orcid.org/0009-0002-4539-6267

Taylor M. Currie − *Department of Chemistry, University of Central Florida, Orlando, Florida 32816, United States;* orcid.org/0009-0008-1256-167X

Eric Bissell − *Department of Materials Science and Engineering, University of Central Florida, Orlando, Florida 32816, United States*

Brian Butkus − *Department of Materials Science and Engineering, University of Central Florida, Orlando, Florida 32816, United States*

Chien-Hsuan Chen − *Department of Materials Science and Engineering, University of Central Florida, Orlando, Florida 32816, United States*

Luis Tomar − *Department of Materials Science and Engineering, University of Central Florida, Orlando, Florida 32816, United States*

Jacob Baillie − *Department of Chemistry, University of Washington, Seattle, Washington 98195-1700, United States*

Daniel R. Gamelin − *Department of Chemistry, University of Washington, Seattle, Washington 98195-1700, United States;* orcid.org/0000-0003-2888-9916

Kristopher O. Davis − *Department of Materials Science and Engineering, University of Central Florida, Orlando, Florida 32816, United States; Resilient Intelligent Sustainable Energy Systems Faculty Cluster, CREOL, the College of Optics and Photonics, and REACT Faculty Cluster, University of Central Florida, Orlando, Florida 32816, United States; Florida Solar Energy Center, University of Central Florida, Cocoa, Florida 32922, United States;* orcid.org/0000-0002-5772-6254

Titel Jurca − *Department of Chemistry, Nano Science and Technology Center, and REACT Faculty Cluster, University of Central Florida, Orlando, Florida 32816, United States;* orcid.org/0000-0003-3656-912X

Complete contact information is available at: https://pubs.acs.org/10.1021/acs.chemmater.4c00667

Notes

The authors declare no competing financial interest.

■ ACKNOWLEDGMENTS

S.N.B. and P.B. acknowledge the funding from the Semiconductor Research Corporation (SRC) under grant no. 3026.001. T.J. and L.T. were supported by National Science Foundation award number 2121953. The Raman system used was acquired under the NSF MRI program award #1920050. The XPS work was supported via NSF MRI award 1726636.

■ REFERENCES

(1) Nakata, K.; Fujishima, A. TiO_2 photocatalysis: Design and applications. *J. Photochem. Photobiol., C* **2012**, *13* (3), 169−189.

(2) Cameron, P. J.; Peter, L. M. Characterization of Titanium Dioxide Blocking Layers in Dye-Sensitized Nanocrystalline Solar Cells. *J. Phys. Chem. B* **2003**, *107* (51), 14394−14400.

(3) Braun, J. H.; Baidins, A.; Marganski, R. E. TiO_2 pigment technology: a review. *Prog. Org. Coat.* **1992**, *20* (2), 105−138.

(4) Morsella, M.; d'Alessandro, N.; Lanterna, A. E.; Scaiano, J. C. Improving the Sunscreen Properties of TiO_2 through an Understanding of Its Catalytic Properties. *ACS Omega* **2016**, *1* (3), 464−469.

(5) Chen, X. B.; Liu, L.; Yu, P. Y.; Mao, S. S. Increasing Solar Absorption for Photocatalysis with Black Hydrogenated Titanium Dioxide Nanocrystals. *Science* **2011**, *331* (6018), 746−750.

(6) Naldoni, A.; Allieta, M.; Santangelo, S.; Marelli, M.; Fabbri, F.; Cappelli, S.; Bianchi, C. L.; Psaro, R.; Dal Santo, V. Effect of Nature and Location of Defects on Bandgap Narrowing in Black TiO_2 Nanoparticles. *J. Am. Chem. Soc.* **2012**, *134* (18), 7600−7603.

(7) Chen, X. B.; Liu, L.; Huang, F. Q. Black titanium dioxide (TiO_2) nanomaterials. *Chem. Soc. Rev.* **2015**, *44* (7), 1861−1885.

(8) Hu, Y. H. A Highly Efficient Photocatalyst - Hydrogenated Black TiO_2 for the Photocatalytic Splitting of Water. *Angew. Chem., Int. Ed.* **2012**, *51* (50), 12410−12412.

(9) Naldoni, A.; Altomare, M.; Zoppellaro, G.; Liu, N.; Kment, S.; Zboril, R.; Schmuki, P. Photocatalysis with Reduced TiO_2: From Black TiO_2 to Cocatalyst-Free Hydrogen Production. *ACS Catal.* **2019**, *9* (1), 345−364.

(10) Liu, X.; Zhu, G.; Wang, X.; Yuan, X.; Lin, T.; Huang, F. Progress in Black Titania: A New Material for Advanced Photocatalysis. *Adv. Energy Mater.* **2016**, *6* (17), 1600452.

(11) Wang, Z.; Yang, C.; Lin, T.; Yin, H.; Chen, P.; Wan, D.; Xu, F.; Huang, F.; Lin, J.; Xie, X.; Jiang, M. H-Doped Black Titania with Very High Solar Absorption and Excellent Photocatalysis Enhanced by Localized Surface Plasmon Resonance. *Adv. Funct. Mater.* **2013**, *23* (43), 5444−5450.

(12) Liu, N.; Schneider, C.; Freitag, D.; Hartmann, M.; Venkatesan, U.; Muller, J.; Spiecker, E.; Schmuki, P. Black TiO_2 Nanotubes: Cocatalyst-Free Open-Circuit Hydrogen Generation. *Nano Lett.* **2014**, *14* (6), 3309−3313.

(13) Shin, J.-Y.; Joo, J. H.; Samuelis, D.; Maier, J. Oxygen-Deficient $TiO_{2-\delta}$ Nanoparticles via Hydrogen Reduction for High Rate Capability Lithium Batteries. *Chem. Mater.* **2012**, *24* (3), 543−551.

(14) Chen, X.; Liu, L.; Liu, Z.; Marcus, M. A.; Wang, W.-C.; Oyler, N. A.; Grass, M. E.; Mao, B.; Glans, P.-A.; Yu, P. Y.; Guo, J.; Mao, S. S. Properties of Disorder-Engineered Black Titanium Dioxide Nanoparticles through Hydrogenation. *Sci. Rep.* **2013**, *3* (1), 1510.
(15) Islam, S. Z.; Reed, A.; Nagpure, S.; Wanninayake, N.; Browning, J. F.; Strzalka, J.; Kim, D. Y.; Rankin, S. E. Hydrogen incorporation by plasma treatment gives mesoporous black TiO_2 thin films with visible photoelectrochemical water oxidation activity. *Microporous Mesoporous Mater.* **2018**, *261*, 35−43.
(16) Binetti, E.; El Koura, Z.; Patel, N.; Dashora, A.; Miotello, A. Rapid hydrogenation of amorphous TiO_2 to produce efficient H-doped anatase for photocatalytic water splitting. *Appl. Catal., A* **2015**, *500*, 69−73.
(17) Sahoo, S. S.; Mansingh, S.; Babu, P.; Parida, K. Black titania an emerging photocatalyst: review highlighting the synthesis techniques and photocatalytic activity for hydrogen generation. *Nanoscale Adv.* **2021**, *3* (19), 5487−5524.
(18) Lu, H.; Zhao, B.; Pan, R.; Yao, J.; Qiu, J.; Luo, L.; Liu, Y. Safe and facile hydrogenation of commercial Degussa P25 at room temperature with enhanced photocatalytic activity. *RSC Adv.* **2014**, *4* (3), 1128−1132.
(19) Naldoni, A.; Allieta, M.; Santangelo, S.; Marelli, M.; Fabbri, F.; Cappelli, S.; Bianchi, C. L.; Psaro, R.; Dal Santo, V. Effect of Nature and Location of Defects on Bandgap Narrowing in Black TiO_2 Nanoparticles. *J. Am. Chem. Soc.* **2012**, *134* (18), 7600−7603.
(20) Zhang, D.; Cong, T.; Xia, L.; Pan, L. Growth of black TiO_2 nanowire/carbon fiber composites with dendritic structure for efficient visible-light-driven photocatalytic degradation of methylene blue. *J. Mater. Sci.* **2019**, *54* (10), 7576−7588.
(21) Li, Z. B.; Bian, H. D.; Xiao, X. F.; Shen, J. D.; Zhao, C. H.; Lu, J.; Li, Y. Y. Defective Black TiO_2 Nanotube Arrays for Enhanced Photocatalytic and Photoelectrochemical Applications. *ACS Appl. Nano Mater.* **2019**, *2* (11), 7372−7378.
(22) Godoy, A.; Pereira, A.; Gomes, M.; Fraga, M.; Pessoa, R.; Leite, D.; Petraconi, G.; Nogueira, A.; Wender, H.; Miyakawa, W.; Massi, M.; Da Silva Sobrinho, A. Black TiO_2 Thin Films Production Using Hollow Cathode Hydrogen Plasma Treatment: Synthesis, Material Characteristics and Photocatalytic Activity. *Catalysts* **2020**, *10* (3), 282.
(23) Ali-Löytty, H.; Hannula, M.; Saari, J.; Palmolahti, L.; Bhuskute, B. D.; Ulkuniemi, R.; Nyyssönen, T.; Lahtonen, K.; Valden, M. Diversity of TiO_2: Controlling the Molecular and Electronic Structure of Atomic-Layer-Deposited Black TiO_2. *ACS Appl. Mater. Interfaces* **2019**, *11* (3), 2758−2762.
(24) George, S. M. Atomic Layer Deposition: An Overview. *Chem. Rev.* **2010**, *110* (1), 111−131.
(25) Profijt, H. B.; Potts, S. E.; van de Sanden, M. C. M.; Kessels, W. M. M. Plasma-Assisted Atomic Layer Deposition: Basics, Opportunities, and Challenges. *J. Vac. Sci. Technol., A* **2011**, *29* (5), 050801.
(26) Kim, H.; Oh, I.-K. Review of plasma-enhanced atomic layer deposition: Technical enabler of nanoscale device fabrication. *Jpn. J. Appl. Phys.* **2014**, *53* (3S2), 03DA01.
(27) Knoops, H. C. M.; Faraz, T.; Arts, K.; Kessels, W. M. M. Status and prospects of plasma-assisted atomic layer deposition. *J. Vac. Sci. Technol., A* **2019**, *37* (3), 030902.
(28) Boris, D. R.; Wheeler, V. D.; Nepal, N.; Qadri, S. B.; Walton, S. G.; Eddy, C. R. The role of plasma in plasma-enhanced atomic layer deposition of crystalline films. *J. Vac. Sci. Technol., A* **2020**, *38* (4), 040801.
(29) Aarik, J.; Aidla, A.; Sammelselg, V.; Uustare, T. Effect of growth conditions on formation of TiO_2-II thin films in atomic layer deposition process. *J. Cryst. Growth* **1997**, *181* (3), 259−264.
(30) Aarik, J.; Aidla, A.; Uustare, T.; Ritala, M.; Leskela, M. Titanium isopropoxide as a precursor for atomic layer deposition: characterization of titanium dioxide growth process. *Appl. Surf. Sci.* **2000**, *161* (3−4), 385−395.
(31) Lim, G. T.; Kim, D. H. Characteristics of TiO_x films prepared by chemical vapor deposition using tetrakis-dimethyl-amido-titanium and water. *Thin Solid Films* **2006**, *498* (1−2), 254−258.
(32) Maeng, W. J.; Kim, H. Thermal and plasma-enhanced ALD of Ta and Ti oxide thin films from alkylamide precursors. *Electrochem. Solid-State Lett.* **2006**, *9* (6), G191−G194.
(33) Aarik, J.; Aidla, A.; Uustare, T. Atomic-layer growth of TiO_2-II thin films. *Philos. Mag. Lett.* **1996**, *73* (3), 115−119.
(34) Rosental, A.; Adamson, P.; Gerst, A.; Koppel, H.; Tarre, A. Atomic layer deposition in traveling-wave reactor: In situ diagnostics by optical reflection. *Appl. Surf. Sci.* **1997**, *112*, 82−86.
(35) Ritala, M.; Leskela, M.; Niinisto, L.; Haussalo, P. Titanium isopropoxide as a precursor in atomic layer epitaxy of titanium dioxide thin films. *Chem. Mater.* **1993**, *5* (8), 1174−1181.
(36) Aghaee, M.; Maydannik, P. S.; Johansson, P.; Kuusipalo, J.; Creatore, M.; Homola, T.; Cameron, D. C. Low temperature temporal and spatial atomic layer deposition of TiO2 films. *J. Vac. Sci. Technol., A* **2015**, *33* (4), 041512.
(37) O'Donnell, S.; Jose, F.; Shiel, K.; Snelgrove, M.; McFeely, C.; McGill, E.; O'Connor, R. Thermal and plasma enhanced atomic layer deposition of ultrathin TiO_2 on silicon from amide and alkoxide precursors: growth chemistry and photoelectrochemical performance. *J. Phys. D: Appl. Phys.* **2022**, *55* (8), 085105.
(38) Xie, Q.; Musschoot, J.; Deduytsche, D.; Van Meirhaeghe, R.; Detavernier, C.; Van den Berghe, S.; Jiang, Y.-L.; Ru, G.-P.; Li, B.-Z.; Qu, X.-P. Growth Kinetics and Crystallization Behavior of TiO_2 Films Prepared by Plasma Enhanced Atomic Layer Deposition. *J. Electrochem. Soc.* **2008**, *155*, H688−H692.
(39) Moulder, J. F.; Stickle, W. F.; Sobol, P. E.; Bomben, K. D. *Handbook of X-Ray Photoelectron Spectroscopy*; Physical Electronics: Eden Prairie, MN, 1995.
(40) Jackman, M. J.; Thomas, A. G.; Muryn, C. Photoelectron Spectroscopy Study of Stoichiometric and Reduced Anatase TiO_2 (101) Surfaces: The Effect of Subsurface Defects on Water Adsorption at Near-Ambient Pressures. *J. Phys. Chem. C* **2015**, *119* (24), 13682−13690.
(41) Su, Y.; Cao, J.; Li, L.; Zhang, G.; Zheng, P. TiO_2 hollow spheres with surface-rich Ti^{3+} under Pd-catalyzed hydrogenation for improved visible-light photocatalysis. *J. Nanopart. Res.* **2019**, *21* (2), 31.
(42) Jayashree, S.; Ashokkumar, M. Switchable Intrinsic Defect Chemistry of Titania for Catalytic Applications. *Catalysts* **2018**, *8* (12), 601.
(43) Rossella, F.; Galinetto, P.; Mozzati, M. C.; Malavasi, L.; Diaz Fernandez, Y.; Drera, G.; Sangaletti, L. TiO_2 thin films for spintronics application: a Raman study. *J. Raman Spectrosc.* **2010**, *41* (5), 558−565.
(44) Ramadan, R.; Manso-Silván, M.; Martín-Palma, R. J. Hybrid porous silicon/silver nanostructures for the development of enhanced photovoltaic devices. *J. Mater. Sci.* **2020**, *55* (13), 5458−5470.
(45) Bhachu, D. S.; Sathasivam, S.; Sankar, G.; Scanlon, D. O.; Cibin, G.; Carmalt, C. J.; Parkin, I. P.; Watson, G. W.; Bawaked, S. M.; Obaid, A. Y.; Al-Thabaiti, S.; Basahel, S. N. Solution Processing Route to Multifunctional Titania Thin Films: Highly Conductive and Photcatalytically Active Nb:TiO_2. *Adv. Funct. Mater.* **2014**, *24* (32), 5075−5085.
(46) Burstein, E. Anomalous Optical Absorption Limit in InSb. *Phys. Rev.* **1954**, *93* (3), 632−633.
(47) Chaukulkar, R. P.; Agarwal, S. Atomic layer deposition of titanium dioxide using titanium tetrachloride and titanium tetraisopropoxide as precursors. *J. Vac. Sci. Technol., A* **2013**, *31* (3), 031509.
(48) Möls, K.; Aarik, L.; Mändar, H.; Kasikov, A.; Niilisk, A.; Rammula, R.; Aarik, J. Influence of phase composition on optical properties of TiO_2: Dependence of refractive index and band gap on formation of TiO_2-II phase in thin films. *Opt. Mater.* **2019**, *96*, 109335.
(49) Wilson, R.; Simion, C.; Blackman, C.; Carmalt, C.; Stanoiu, A.; Di Maggio, F.; Covington, J. The Effect of Film Thickness on the Gas Sensing Properties of Ultra-Thin TiO_2 Films Deposited by Atomic Layer Deposition. *Sensors* **2018**, *18* (3), 735.
(50) Martin, N.; Besnard, A.; Sthal, F.; Vaz, F.; Nouveau, C. The contribution of grain boundary barriers to the electrical conductivity of titanium oxide thin films. *Appl. Phys. Lett.* **2008**, *93* (6), 064102.

https://doi.org/10.1021/acs.chemmater.4c00667
Chem. Mater. XXXX, XXX, XXX−XXX

(51) Bally, A. R.; Korobeinikova, E. N.; Schmid, P. E.; Lévy, F.; Bussy, F. Structural and electrical properties of Fe-doped thin films. *J. Phys. D: Appl. Phys.* **1998**, *31* (10), 1149−1154.
(52) Lü, X.; Chen, A.; Luo, Y.; Lu, P.; Dai, Y.; Enriquez, E.; Dowden, P.; Xu, H.; Kotula, P. G.; Azad, A. K.; Yarotski, D. A.; Prasankumar, R. P.; Taylor, A. J.; Thompson, J. D.; Jia, Q. Conducting Interface in Oxide Homojunction: Understanding of Superior Properties in Black TiO_2. *Nano Lett.* **2016**, *16* (9), 5751−5755.
(53) Rahtu, A.; Ritala, M. Reaction Mechanism Studies on Titanium Isopropoxide-Water Atomic Layer Deposition Process. *Chem. Vap. Depos.* **2002**, *8* (1), 21.
(54) Dufond, M. E.; Diouf, M. W.; Badie, C.; Laffon, C.; Parent, P.; Ferry, D.; Grosso, D.; Kools, J. C. S.; Elliott, S. D.; Santinacci, L. Quantifying the Extent of Ligand Incorporation and the Effect on Properties of TiO_2 Thin Films Grown by Atomic Layer Deposition Using an Alkoxide or an Alkylamide. *Chem. Mater.* **2020**, *32* (4), 1393−1407.
(55) Reinke, M.; Kuzminykh, Y.; Hoffmann, P. Surface Reaction Kinetics of Titanium Isopropoxide and Water in Atomic Layer Deposition. *J. Phys. Chem. C* **2016**, *120* (8), 4337−4344.
(56) Rai, V. R.; Agarwal, S. Surface Reaction Mechanisms during Plasma-Assisted Atomic Layer Deposition of Titanium Dioxide. *J. Phys. Chem. C* **2009**, *113* (30), 12962−12965.
(57) Potts, S. E.; Keuning, W.; Langereis, E.; Dingemans, G.; van de Sanden, M. C. M.; Kessels, W. M. M. Low Temperature Plasma-Enhanced Atomic Layer Deposition of Metal Oxide Thin Films. *J. Electrochem. Soc.* **2010**, *157* (7), P66.
(58) Lakshmanan, S. K.; Gill, W. N. A novel model of hydrogen plasma assisted chemical vapor deposition of copper. *Thin Solid Films* **1999**, *338* (1−2), 24−39.
(59) Cho, S.-I.; Chung, C.-H.; Moon, S. H. Surface decomposition mechanism of $Ti(OC_3H_7)_4$ on a platinum surface. *Thin Solid Films* **2002**, *409* (1), 98−104.
(60) Pham, H. H.; Wang, L. W. Oxygen vacancy and hole conduction in amorphous TiO_2. *Phys. Chem. Chem. Phys.* **2015**, *17* (1), 541−550.

https://doi.org/10.1021/acs.chemmater.4c00667
Chem. Mater. XXXX, XXX, XXX−XXX